ISSN: 2414-1895 DOI: 10.6919/ICJE.202405_10(5).0016

Nonlinear Dynamics Analysis of Face-gear Transmission System Considering Thermal Elasto-hydrodynamic Lubrication

Wang Li[1, a], Linjie Zhang[1, b], Yuqiang Cai[1, c], Pengyuan Qiu[2, d], and Jingzi Zhang[1, e]

[1] School of mechanical engineering, North China University of Science and Technology, Tangshan 063210, China

[2] School of Aerospace Engineering, Taizhou University, Taizhou 300072, China

[a]Lw201906@ncst.edu.cn, [b]qpengyuan0614@163.com, [c]caiyq@ncst.edu.cn, [d]qpengyuan0614@163.com, [e]zhang.jingzi@163.com

Abstract

Face gear drives play an increasingly important role in the transmission systems of helicopter. Concentrated parameter dynamic model with 6 degrees of freedom (6-DOF) taking into account nonlinear backlash, time-varying stiffness of meshing, and coefficient of friction coupling has been developed for face-gear transmission systems under thermal elasto-hydrodynamics lubrication (EHL) conditions. The dynamic properties of the face-gear transmission system were analyzed using bifurcation diagrams. The effect of pinion rotation speed and support rigidity on the dynamic response of the face-gear transmission system was studied in detail using numerical methods. Numerical examples reveal several dynamic evolutionary mechanisms and kinetic states, including period 1, period 2, chaos and quasiperiodic motion. Some research results are useful for vibration control and dynamic design of the face-gear transmission system of helicopters.

Keywords

Face Gear; Helicopter; Dynamic Model; Elasto-hydrodynamic Lubrication; LTCA.

1. Introduction

Face-gear drives play an increasingly important role in helicopter power transmission systems due to their high torque splitting capability and sensitivity to misalignment errors [1-3]. Helicopter transmission systems are characterized by high speeds, high loads, and complex operating environments, and are prone to gear damage due to intense vibration. Therefore, it is essential to develop an accurate and reliable dynamic model of the gear transmission system to investigate the failure mechanism. In fact, the study of the dynamic behavior of gear transmission systems is one of the most important aspects of power transmission design.

Nonlinear dynamic properties are one of the focus of research in gearing systems. Theodossiades [4] investigated the periodic steady-state response of a gear pair system involving time-dependent periodic meshing rigidity and backlash. The periodic steady state was then identified by employing techniques that can be applied to oscillators with periodic coefficients and piecewise linear systems.

By thoroughly studying the dynamic behavior of gear systems, the consideration of nonlinear parameters is becoming more and more sophisticated. Gora [5] presented a modified dynamic model to investigate the dynamic response of a spur gear system, including the flash temperature of the contact surface. Paulis [6] studied dynamic behavior of a hypoid gear pair in an automobile, and his research was based on a thermal three-body dynamic model.

ISSN: 2414-1895 DOI: 10.6919/ICJE.202405_10(5).0016

Face gear drives have been used in helicopter transmissions since the 1990s. Wang [7] proposed a dynamic model of flexion, torsion, and axial-coupled transmission system using centralized parameter theory. The nonlinear dynamic response of the face gear drive system was investigated by Wang using a six-degree-of-freedom dynamic model that takes into account backlash, time-varying stiffness of the meshing arm, time-varying meshing force, and the effects of correction [8]. Hura [9] presented a dynamic model of 14 degrees of freedom of a face-gear rotor system.

In contrast to other types of gear systems, research on the dynamic behavior of gear-gear transmission systems is limited. Face gear drives are promising for use in helicopter transmissions. It is therefore essential to clarify the essential relationship between these factors and the dynamic behavior of the gear transmission system.

2. Models for the Face-gear Transmission System

2.1 Dynamic Model of Face-gear Transmission System

For convenience of calculation, the gear body is regarded as a rigid disk with the same moment of inertia. The teeth meshes are modeled as nonlinear spring damper elements acting along line of action (LOA), and the bearings are simplified as linear spring damper elements. The dynamic model of face-gear transmission system is depicted in Figure. 1.

Herein, $\mu(t)$ represents the nonlinear friction that tangent to the contact tooth surfaces and perpendicular to the acting line at the instantaneous contact point, b denotes half of the total backlash, $k_m(t)$ and c_m are the time varing meshing stiffness and viscus mesh damping coefficient respectively, $e(t)$ represents the time varying static transmission error.

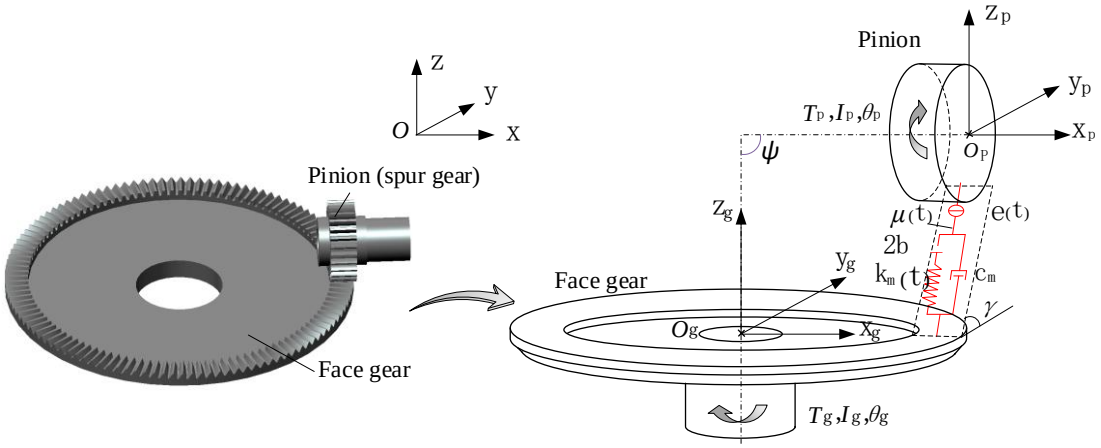

Figure 1. The dynamic model of face-gear transmission system

In addition, the generalized displacement vector is defined by:

$$\boldsymbol{\delta} = \left\{ y_p, z_p, w_p, y_g, z_g, w_g \right\}^T \tag{1}$$

The transmission error is:

$$\delta(t) = \mathbf{q} \cdot \boldsymbol{\delta} - e(t) \tag{2}$$

where $\mathbf{q} = [\cos\gamma, \sin\gamma, 1, -\cos\gamma, -\sin\gamma, -\cos\gamma]$.

The nonlinear gear backlash is:

ISSN: 2414-1895 DOI: 10.6919/ICJE.202405_10(5).0016

$$f(x)=\begin{cases}x-b & x>b\\ 0 & -b<x<b\\ x+b & x<-b\end{cases} \tag{3}$$

The meshing force is:

$$F_m(t)=f\left(\delta(t)\right)\cdot k_m(t)+\dot{f}\left(\delta(t)\right)\cdot c_m(t) \tag{4}$$

The equations of the 6-DOF dynamic model can be derived as:

$$\begin{cases} m_p\ddot{y}_p+c_p^y\dot{y}_p+k_p^y y_p=F_m(t)(\cos\gamma-\sum_{n=1}^{N}\zeta_n\xi_n\mu_n(t)\sin\gamma)\\ m_p\ddot{z}_p+c_p^z\dot{z}_p+k_p^z z_p=F_m(t)(\sin\gamma-\sum_{n=1}^{N}\zeta_n\xi_n\mu_n(t)\cos\gamma)\\ I_p\ddot{w}_p/R_p=T_p-F_m(t)(R_p\cos\gamma+\sum_{n=1}^{N}\zeta_n\xi_n\mu_n(t)r_p^n(t)\sin\gamma)\\ m_g\ddot{y}_g+c_g^y\dot{y}_g+k_g^y y_g=-F_m(t)(\cos\gamma-\sum_{n=1}^{N}\zeta_n\xi_n\mu_n(t)\sin\gamma)\\ m_g\ddot{z}_g+c_g^z\dot{z}_g+k_g^z z_g=-F_m(t)(\sin\gamma-\sum_{n=1}^{N}\zeta_n\xi_n\mu_n(t)\cos\gamma)\\ I_g\ddot{w}_g/R_g=-T_g+F_m(t)(R_g\cos\gamma+\sum_{n=1}^{N}\zeta_n\xi_n\mu_n(t)r_g^n(t)\sin\gamma)\end{cases} \tag{5}$$

where m_i is the mass of gear i, I_i is the mass moment of inertia of gear i, k_i^j and c_i^j are the average supporting stiffness and bearing damping of gear i respectively along j direction ($j=y$, z), $r_i^n(t)$ is the radius of instantaneous contact point of contact tooth pair n of gear i, ξ_n represents the load sharing ratio of contact tooth pair n, and N denotes the total number of contact tooth pairs at an instantaneous contact.

The non-demensional time ε is defined by $\varepsilon=t/\omega_n$, where ω_n is the meshing period of gear teeth. The non-demensional displacements, velocities and accelerations can be expressed as:

$$\begin{aligned} &Y_p=y_p/b_l, Z_p=z_p/b_l, W_p=w_p/b_l, Y_g=y_g/b_l, Z_g=z_g/b_l\\ &\dot{Y}_p=\dot{y}_p\omega_n/b_l, \dot{Z}_p=\dot{z}_p\omega_n/b_l, \dot{W}_p=\dot{w}_p\omega_n/b_l, \dot{Y}_g=\dot{y}_g\omega_n/b_l, \dot{Z}_g=\dot{z}_g\omega_n/b_l, \dot{W}_g=\dot{w}_g\omega_n/b_l\\ &\ddot{Y}_p=\ddot{y}_p\omega_n^2/b_l, \ddot{Z}_p=\ddot{z}_p\omega_n^2/b_l, \ddot{W}_p=\ddot{w}_p\omega_n^2/b_l, \ddot{Y}_g=\ddot{y}_g\omega_n^2/b_l, \ddot{Z}_g=\ddot{z}_g\omega_n^2/b_l, \ddot{W}_g=\ddot{w}_g\omega_n^2/b_l \end{aligned} \tag{6}$$

The non-demensional form of the dynamic modle is

$$\begin{cases} \ddot{Y}_p+C_p^y\dot{Y}_p+K_p^y Y_p=F_p^y\\ \ddot{Z}_p+C_p^z\dot{Z}_p+K_p^z Z_p=F_p^z\\ \ddot{Y}_g+C_g^y\dot{Y}_g+K_g^y Y_g=F_g^y\\ \ddot{Z}_g+C_g^z\dot{Z}_g+K_g^z Z_g=F_g^z\\ \ddot{W}_p=F_p^w, \ddot{W}_g=F_g^w\end{cases} \tag{7}$$

ISSN: 2414-1895 DOI: 10.6919/ICJE.202405_10(5).0016

Where:

$$F_p^y = F(\varepsilon\omega_n)(\cos\gamma - \sum_{n=1}^{N}\zeta_n\xi_n\mu_n(\varepsilon\omega_n)\sin\gamma)/(m_p b_l/\omega_n^2), F_g^y = -F_p^y$$

$$F_p^z = F(\varepsilon\omega_n)(\sin\gamma - \sum_{n=1}^{N}\zeta_n\xi_n\mu_n(\varepsilon\omega_n)\cos\gamma)/(m_p b_l/\omega_n^2), F_g^z = -F_p^z$$

$$F_p^w = (T_p - F(\varepsilon\omega_n)(R_p\cos\gamma - \sum_{n=1}^{N}\zeta_n\xi_n\mu_n(\varepsilon\omega_n)r_p^n(\varepsilon\omega_n)\sin\gamma))/(I_p b_l/\omega_n^2/R_p)$$

$$F_g^w = (-T_g + F(\varepsilon\omega_n)(R_g\cos\gamma + \sum_{n=1}^{N}\zeta_n\xi_n\mu_n(\varepsilon\omega_n)r_g^n(\varepsilon\omega_n)\sin\gamma))/(I_g b_l/\omega_n^2/R_g)$$

$$C_p^y = c_p^y/(m_p/\omega_n), C_p^z = c_p^z/(m_p/\omega_n), C_g^y = c_g^y/(m_p/\omega_n), C_g^z = c_g^z/(m_p/\omega_n)$$

$$K_p^y = k_p^y/(m_p/\omega_n^2), K_p^z = k_p^z/(m_p/\omega_n^2), K_g^y = k_g^y/(m_p/\omega_n^2), K_g^z = k_g^z/(m_p/\omega_n^2)$$

2.2 EHL Model

2.2.1 Contact Model

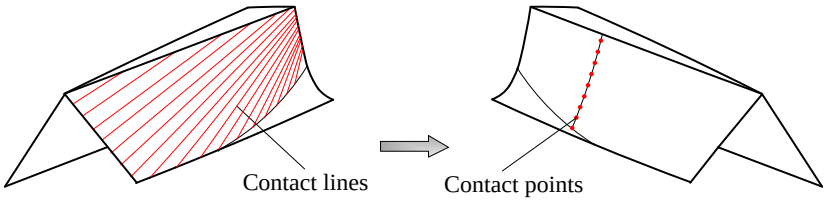

Figure 2. Localization of contact pattern

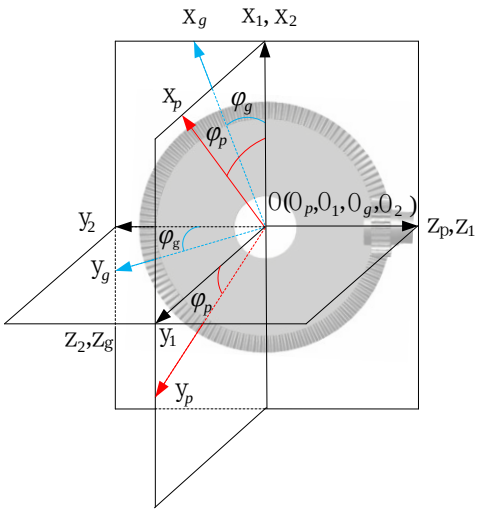

Figure 3. Meshing model of face-gear transmission

Accordingly, the shaper is designed with an increased tooth number, generally $N_s - N_p = 1$ to 3, to localize the contact pattern. Figure. 2 illustrates the localization of contact pattern of face-gear transmission. Denote the surfaces of shaper, face gear and pinion which mesh simultaneously by Σ_s, Σ_g and Σ_p respectively. The surfaces Σ_s and Σ_g are in line contact at every instant, the surfaces Σ_s and Σ_p are in line contact at every instant. For $N_s > N_p$, whereas, the surfaces Σ_g and Σ_p are in point contact at every instant.

To localize the contact pattern, the tooth number of shaper is larger than that of pinion. Thus, the mounting position of pinion is lower than that of shaper. The tooth surfaces of pinion and face gear

ISSN: 2414-1895 DOI: 10.6919/ICJE.202405_10(5).0016

are in point contact at every instant and the contact geometry parameters that are needed for thermal EHL can be obtained from unloaded tooth contact analysis. The assembly of face gear that meshes with a spur gear is schematically illustrated in Figure. 3 in which four coordinate systems are contained. The fixed coordinate systems S_1 and S_2 that are connected to the frame of machine rigidly are the reference of pinion and face gear respectively. And S_2 is also the global coordinate system of this meshing model. The moving coordinate systems S_p and S_g are fixed to pinion and face gear respectively. According to the meshing theory, the surfaces of pinion and face gear is in continuous tangency, and the equivalence of position vector and collinear surface normal is observed at the instantaneous contact point in the fixed coordinate system S_2.

Thus, the continuous tangency conditions of the surfaces of pinion and face gear in the global coordinate system S_2 can be expressed as:

$$\begin{cases} \mathbf{r}_p^{(2)}\left(u_p, l_p, \phi_p\right) - \mathbf{r}_g^{(2)}\left(u_s, l_s, \phi_s, \phi_g\right) = 0 \\ \mathbf{n}_p^{(2)}\left(u_p, l_p, \phi_p\right) - \mathbf{n}_g^{(2)}\left(u_s, l_s, \phi_s, \phi_g\right) = 0 \\ f_{\mathbf{nv}}\left(u_s, l_s, \phi_s\right) = \mathbf{n}_s^{(2)} \cdot \mathbf{v}_{s,f}^{(2)} = 0 \end{cases} \tag{8}$$

where $\mathbf{r}_i^{(2)}$ and $\mathbf{n}_i^{(2)}$ denote the position vector and surface normal of gear i respectively, $\mathbf{n}_s^{(2)}$ represents the surface normal of shaper, the superscript (2) represents the global coordinate system S_2, $\mathbf{v}_{s,f}^{(2)}$ is the relative surface velocity between shaper and face gear at the instantaneous contact point. Eq. (8) represents six independent nonlinear equations with seven variables. Therefore, once the rotational angle ϕ_p of pinion is given, the other six variables can be obtained from the nonlinear equation system.

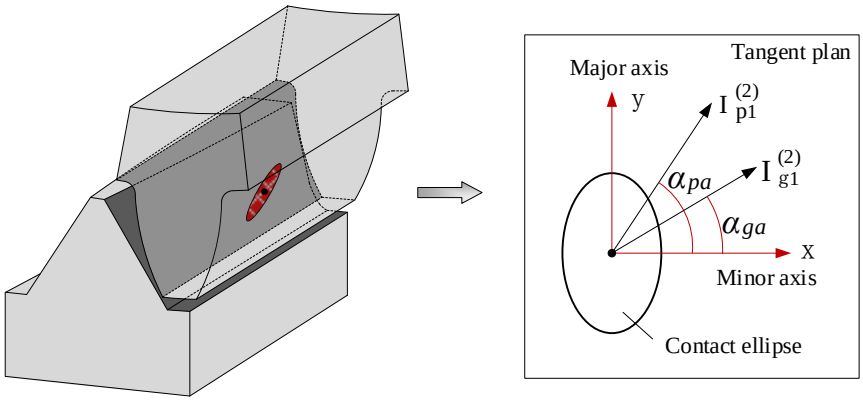

Figure 4. Contact ellipse of pinion and face gear

The contact of tooth surfaces can be equivalent to two ellipsoids in contact [10]. And for the convenience of calculation, the contact of two ellipsoids are furthermalre equivalent to the contact of an ellipsoid with a semi-infinite rigid plane. Due to the elastic deformations of tooth surfaces, the instantaneous contact point of tooth surfaces extends into an elliptical contact area, and the symmetry center of the contact ellipse coincides with the theoretical tangent contact point. The contact path is a group of contact ellipses. Figure. 4 illustrates the Hertzian contact ellipse in the tangent plane, where $\mathbf{I}_p^{(2)}, \mathbf{I}_g^{(2)}$ represent the first principal directions of the contacted tooth surfaces of pinion and face gear respectively at the instantaneous contact point.

Thus, the equivalent radii of contact tooth pair can be expressed by:

ISSN: 2414-1895 DOI: 10.6919/ICJE.202405_10(5).0016

$$\begin{cases} R_a = 1/(K_{p1}\cos^2\alpha_{pa} + K_{p2}\sin^2\alpha_{pa} + K_{g1}\cos^2\alpha_{ga} + K_{g2}\sin^2\alpha_{ga}) \\ R_b = 1/(K_{p1}\sin^2\alpha_{pa} + K_{p2}\cos^2\alpha_{pa} + K_{g1}\sin^2\alpha_{ga} + K_{g2}\cos^2\alpha_{ga}) \end{cases} \tag{9}$$

where K_{i1} and K_{i2} are the first and second principal curvature of gear i at the instantaneous contact point. α_{ia} represents the angle between the principal direction and the minor axis of the contact ellipse of gear i at the instantaneous contact point.

The equivalent elastic modulus can be expressed as:

$$\frac{1}{E} = \frac{1}{2}\left(\frac{1-\upsilon_p^2}{E_p} + \frac{1-\upsilon_g^2}{E_g}\right) \tag{10}$$

where E_p and E_g is the elastic modulus of the spur gear and the face gear respectively, υ_p and υ_g are the Poisson's ratio of pinion and the face gear respectively.

The velocity vectors of the contact points on the tooth surfaces of pinion and face gear in their own fixed coordinate system can be derived by:

$$\begin{cases} \mathbf{v}_p^{(p)} = \omega_p\left(j_p^{(p)} \times \mathbf{r}_p^{(p)}\right) \\ \mathbf{v}_g^{(g)} = \omega_g\left(j_g^{(g)} \times \mathbf{r}_g^{(g)}\right) \end{cases} \tag{11}$$

where $\mathbf{v}_i^{(i)}$ represents the velocity vector of contact point on the tooth surface of gear i in coordinate system S_i, the superscript (i) represents the coordinate system S_i, $j_i^{(i)}$ represents the unit axis vector of gear i, ω_i and $\mathbf{r}_i^{(2)}$ are the angular velocity vectors and position vectors of the instantaneous contact point in the global fixed coordinate systems S_2.

By coordinate transformation, the velocity vectors in tangent plan can be represented in S_2 as:

$$\begin{cases} \mathbf{v}_{tp}^{(2)} = \mathbf{M}_{2p}\left[\mathbf{v}_p^{(p)} - \left(\mathbf{v}_p^{(p)} \cdot \mathbf{n}_p^{(p)}\right)\mathbf{n}_p^{(p)}\right] \\ \mathbf{v}_{tg}^{(2)} = \mathbf{M}_{2g}\left[\mathbf{v}_g^{(g)} - \left(\mathbf{v}_g^{(g)} \cdot \mathbf{n}_g^{(g)}\right)\mathbf{n}_g^{(g)}\right] \end{cases} \tag{12}$$

where $\mathbf{M}_{2i}$ is the coordinate transformation matrix from S_i to S_2.

By projecting to the major and minor axes, the magnitudes of velocities can be expressed as:

$$\begin{cases} u_p = \mathbf{v}_{tp}^{(2)} \cdot \boldsymbol{\eta}^{(2)} \\ v_p = \mathbf{v}_{tp}^{(2)} \cdot \boldsymbol{\xi}^{(2)} \\ u_g = \mathbf{v}_{tg}^{(2)} \cdot \boldsymbol{\eta}^{(2)} \\ v_g = \mathbf{v}_{tg}^{(2)} \cdot \boldsymbol{\xi}^{(2)} \end{cases} \tag{13}$$

where $\boldsymbol{\eta}^{(2)}$ and $\boldsymbol{\xi}^{(2)}$ are the unit vectors along of the major and minor axes of contact ellipse.

Thus, the entraining and sliding velocities of the face-gear transmission are derived as follows:

ISSN: 2414-1895 DOI: 10.6919/ICJE.202405_10(5).0016

$$\begin{cases} u = \left(u_p + u_p\right)/2 \\ v = \left(v_p + v_g\right)/2 \\ S_u = 2\left(u_p - u_g\right)\left(u_p + u_g\right) \\ S_v = 2\left(v_p - v_g\right)\left(v_p + v_g\right) \end{cases} \tag{14}$$

2.2.2 Basic Equations

In this section, only a brief illustration of the basic lubrication equations is presented. In the elliptical contact area, the oil pressure is governed by the Reynolds equation. The general form of the equation with two directions of lubricant entrainment for the steady-state thermal EHL problem in point contacts can be expressed as [11].

$$\frac{\partial}{\partial x}\left[\left(\frac{\rho}{\eta}\right)_e h^3 \frac{\partial p}{\partial x}\right] + \frac{\partial}{\partial y}\left[\left(\frac{\rho}{\eta}\right)_e h^3 \frac{\partial p}{\partial y}\right] = 12u\frac{\partial}{\partial x}\left(\rho_x^* h\right) + 12v\frac{\partial}{\partial y}\left(\rho_y^* h\right) \tag{15}$$

where $(\rho/\eta)_e$, ρ_x^* and ρ_y^* are the equivalent parameters in terms of non-Newton oil, which were defined in Ref. [12], p represents the oil pressure distribution in solution domain.

The film thickness is represented as:

$$h(x,y) = h_0 + \frac{x^2}{2R_x} + \frac{y^2}{2R_y} + \delta(x,y) \tag{16}$$

where h_0 is a constant and $\delta(x,y)$ is the localized deformation of the instant contact area, which can be represented as:

$$\delta(x,y) = \frac{2}{\pi E'}\iint_\Omega \frac{p(x',y')}{\sqrt{(x-x')^2 + (y-y')^2}}dx'dy' \tag{17}$$

where E' represents comprehensive elastic modulus.

The lubricant viscosity is derived Roelands model.

$$\eta = \eta_0 \exp\left\{A_1\left[-1 + \left(1 + A_2 p\right)^{z_0}\left(A_3 T - A_4\right)^{-s_0}\right]\right\} \tag{18}$$

where $A_1 = \ln\eta_0 + 9.67$, $A_2 = 5.1\times10^{-9}$, $A_3 = 1/(T_0 - 138)$, $A_4 = 138A_3$, $z_0 = \alpha/(A_1A_2)$ and $s_0 = \beta/(A_1A_3)$.

The lubricant density is derived from Dowson-Higginson model.

$$\rho = \rho_0\left[1 + \frac{C_1 p}{1 + C_2 p} - C_3\left(T - T_0\right)\right] \tag{19}$$

where $C_1 = 0.6\times10^{-9}\,\mathrm{Pa}^{-1}$, $C_2 = 1.7\times10^{-9}\,\mathrm{Pa}^{-1}$, $C_3 = 0.00065\,\mathrm{K}^{-1}$.

The load of the contact tooth pair that obtained from Sec. 2.2.1 is in balance with the integral of pressure over the solution domain Ω.

ISSN: 2414-1895 DOI: 10.6919/ICJE.202405_10(5).0016

$$F = \iint_{\Omega} p(x,\ y)dxdy \tag{20}$$

Ignoring the gradient of oil film pressure along the film thickness and the heat conduction, the energy equation for flash temperature is as follows:

$$c_f\left(\rho u\frac{\partial T}{\partial x}+\rho v\frac{\partial T}{\partial y}-\left(\frac{\partial}{\partial x}\int_0^z \rho u dz'+\frac{\partial}{\partial y}\int_0^z \rho v dz'\right)\frac{\partial T}{\partial z}\right)=k_f\frac{\partial^2 T}{\partial z^2}-\frac{T}{\rho}\frac{\partial \rho}{\partial T}\left(u\frac{\partial p}{\partial x}+v\frac{\partial p}{\partial y}\right)+\eta_x^*\left(\frac{\partial u}{\partial z}\right)^2+\eta_y^*\left(\frac{\partial v}{\partial z}\right)^2 \tag{21}$$

The energy equations for the flash temperature inside the solid are represented as

$$\begin{cases} c_p\rho_p u_p\dfrac{\partial T}{\partial x}=k_p\dfrac{\partial^2 T}{\partial z_p^2} \\ c_g\rho_g u_g\dfrac{\partial T}{\partial x}=k_g\dfrac{\partial^2 T}{\partial z_g^2} \end{cases} \tag{22}$$

The friction coefficient is derived by:

$$f=\left(\sqrt{\left(\iint_{\Omega}\tau_{px}(x,\ y)dxdy\right)^2+\left(\iint_{\Omega}\tau_{py}(x,\ y)dxdy\right)^2}+\sqrt{\left(\iint_{\Omega}\tau_{gx}(x,\ y)dxdy\right)^2+\left(\iint_{\Omega}\tau_{gy}(x,\ y)dxdy\right)^2}\right)/F \tag{23}$$

where τ_{ix} and τ_{iy} represent the shear stresses of the two contacted surfaces along x and y directions respectively.

2.3 Thermal EHL-based Time Varying Meshing Stiffness and Friction Coefficient

2.3.1 LTCA under Thermal EHL Condition

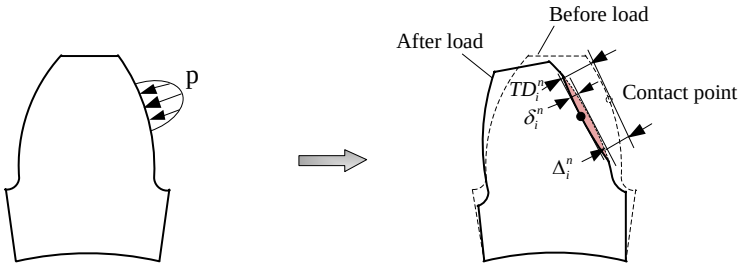

Figure 5. Global deformation and local deformation of gear tooth under thermal EHL condition

To analysis the dynamic behaviors of the face-gear transmission under thermal EHL condition, a LTCA method that with accurate results and high efficiency is needed [13-15]. An accurate and efficient LTCA model under thermal EHL condition is proposed in this section. The total deformation of the contact point is a sum of the global and local deformation of the contact tooth pair, which can be expressed as

$$TD_n=\delta_p^n+\Delta_p^n+\delta_g^n+\Delta_g^n \tag{24}$$

where n represents the number of the contact tooth pair, δ_i^n is the local deformation, Δ_i^n is the global deformation of gear i.

ISSN: 2414-1895 DOI: 10.6919/ICJE.202405_10(5).0016

Accordingly, the local deformation is the results of oil film pressure and flash temperature acting on the contact tooth pair [28]. The tooth deformation that resulting from the oil film pressure is represented as Eq. (17). The tooth deformation δ_{Ti}^{n} resulting from the flash temperature [17] can be represented as:

$$\delta_{Ti}^{n}=\frac{-\Delta t_i \lambda r_{bi}^{2}\left[l_i / r_{bi}-2\left(\mathrm{inv}\alpha_{ki}-\mathrm{inv}\alpha_n\right)\right]}{2\left[r_{bi}+\Delta t_i \lambda r_{bi}\left(1-\cos\alpha_{ki}\right)\right]} \tag{25}$$

Herein, Δt_i is the temperature rise of the tooth surface of gear i, l_i represents the tooth thickness of the gear i at the instantaneous contact point, λ represents the linear expansion of material, α_{ki} represents the press angle of gear i at the instantaneous contact point, r_{bi} is the equivalent base radius of gear i.

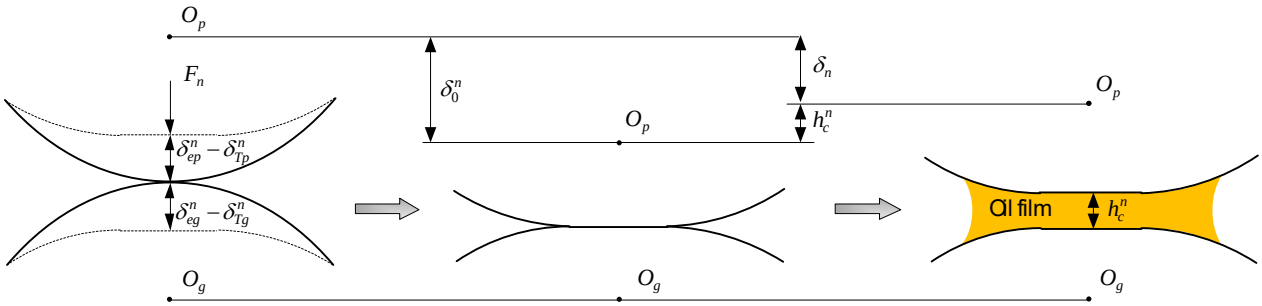

Figure 6. Local deformation under thermal EHL condition

The local deformation of contact tooth pair is illustrated in Figure.6. Thus, the normal approaching distance of two the points (O_p, O_g) on the contact tooth pair which have no elastic deformation can be expressed as:

$$\delta_n=\delta_0^n-h_c^n \tag{26}$$

where δ_0^n ($\delta_0^n=\delta_{ep}^n-\delta_{Tp}^n+\delta_{eg}^n-\delta_{Tg}^n$) represents the local deformation of contact tooth pair n, δ_{ei}^n represents the elastic tooth profile deformation under oil film pressure of gear i, δ_{Ti}^n is the tooth profile deformation result from the flash temperature of gear i, h_c^n denotes the thickness of the oil film in the symmetry center of the instantaneous contact ellipse.

The oil film pressure is in balance with the applied load on the tooth pair:

$$F_n=\iint_{\Omega} p(x,y)\,dxdy \tag{27}$$

where Ω is the solution domain.

When two or more gear tooth pairs are in contact at the instantaneous contact, the total deformation of each contact tooth pair should be equal in order to ensure the continuity of contact between each contact tooth pair. This deformation compatibility relationship can be expressed as:

ISSN: 2414-1895 DOI: 10.6919/ICJE.202405_10(5).0016

$$\delta_n + \Delta_n = C \tag{28}$$

where C is a constant number.

And the load equilibrium condition of all the contact tooth pairs can be expressed as:

$$F_m = \sum_{n=1}^{N} F_n \tag{29}$$

where N is the total number of the contact tooth pairs.

The global deformation δ_n and local deformation Δ_n are functions of F_n. There are N unknown variables (F_n) as the contact tooth pair number is N. Since the total number of equations of Eq. (28) and Eq. (29) is also N, the LTCA problem can be solved. By applying the thermal EHL method to calculate the local deformation, the complicated linear program method in [12] is avoid.

2.3.2 Time Varying Meshing Stiffness and Friction Coefficient

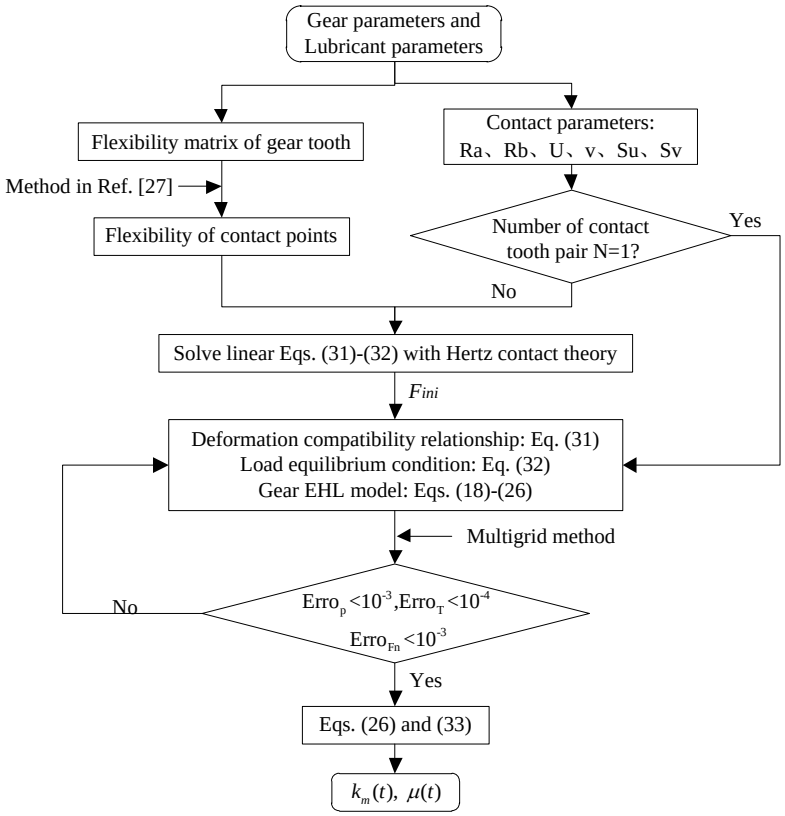

Figure 7. Flow chart for calculating the time varying meshing stiffness and friction coefficient under thermal EHL condition

The time varying meshing stiffness and friction coefficient under thermal EHL condition can be calculated in Figure. 7. The gear design parameters and material parameters, which are the input parameters of this flow chart, are listed in Table 1. The contact model is discussed in Sec. 2.2.1 provides contact geometry parameters including velocities and radii for thermal EHL model. Meantime, in order to obtain the global flexibility of gear tooth, the elastic deformation of contact point will be divided into global deformation and local deformation [27]. Then, to obtain the load of each contact tooth pair, the number of contact tooth pair at an instantaneous contact needs to be determined. When the number of contact tooth pair is equal to 1, the load on gear tooth pair is the full load that the system transmitted. Otherwise, the load of each contact tooth pair must be determined

ISSN: 2414-1895 DOI: 10.6919/ICJE.202405_10(5).0016

by Eq. (28) and Eq. (29). The initial load F_{ini} of each contact tooth pair was calculated based on Hertzian contact theory rather than EHL to facilitate convergence. The above provide the geometric parameters and load for the thermal EHL model that established in Sec. 2.2.2.

The load vector $\mathbf{P}$ and deformation vector $\boldsymbol{\delta}+\boldsymbol{\Delta}$ are obtained by solving Eq. (28) and Eq. (29) in one meshing circle. Accordingly, the time varying meshing stiffness can be represented by:

$$k_m = \frac{\mathbf{P}}{\boldsymbol{\delta}+\boldsymbol{\Delta}} \tag{30}$$

In the processing of the calculation of LTCA under thermal EHL condition, the tooth deformation is made up of three parts, namely, global deformation, local deformation under oil pressure and tooth profile deformation resulting from flash temperature. The design parameters of the face-gear transmission are illustrated in Table 1. Based on the calculation of Sec. 2.3.1, the time varying meshing stiffness in one meshing circle is illustrated in Figure. 8. The friction coefficient of each instant contact can be obtained by Eq. (23). The time varying meshing friction coefficient in one meshing circle is illustrated in Figure. 9.

Table 1. The parameters of face-gear transmission system

Material parameters	**Value**	**Gear design parameters**	**Value**
Density of gears $\rho_{p,g}$ (kg/m^3)	7850	Tooth number of pinion z_p	23
Elastic modulus of gears $E_{p,g}$ (Pa)	2.1×10^{11}	Tooth number of face gear z_g	86
Poisson ratio of gears $v_{p,g}$	0.3	Modulus m (mm)	4
Specific heat of gears $c_{p,g}$ ($J/(kg\cdot℃)$)	470	Tooth width B (mm)	25
Thermal conductivity of gears $k_{p,g}$ ($W/(m\cdot℃)$)	46	Pressure angle α_n (deg)	25
Ambient temperature T_0 (℃)	40	Inner radius of face gear r_{in} (mm)	164
Viscosity-pressure coefficient α (m^2/N)	2.2×10^{-8}	Outer radius of face gear r_{out} (mm)	189
Ambient density of lubricant ρ_0 (kg/m^3)	870	Input torque T_{in} ($N\cdot m$)	400
Ambient viscosity of lubricant η_0 ($Pa\cdot s$)	0.04	Rotational speed of pinion n_p (rad/min)	3000
Specific heat of lubricant c_f ($J/(kg\cdot℃)$)	2000		
Thermal conductivity of lubricant k_f ($W/(m\bullet℃)$)	0.14		
Viscosity-temperature coefficient β_T (K^{-1})	0.0476		
Characteristic shear stress τ_0 (Pa)	1×10^7		

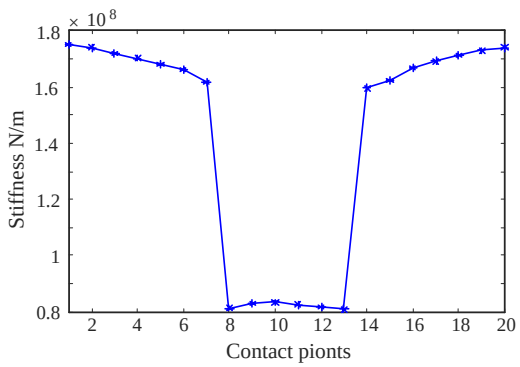

Figure 8. Time varying meshing stiffness in one meshing circle

ISSN: 2414-1895 DOI: 10.6919/ICJE.202405_10(5).0016

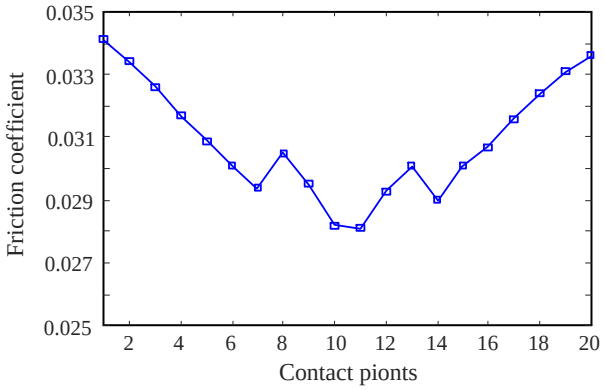

Figure 9. friction coefficient in one meshing circle

3. Nonlinear Dynamic Responses

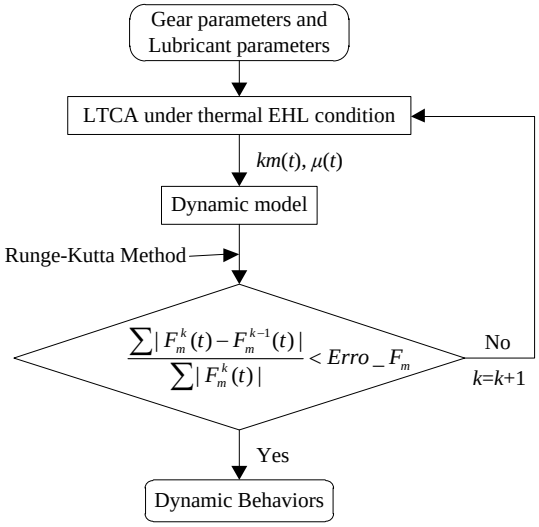

Figure 10. Computation procedure of the dynamic response of the face-gear transmission system

As illustrated in Figure. 10, an iterative loop is organized to calculate the dynamic responses by adopting Runge-Kutta method and multigrid method. The gear design parameters and material parameters are prepared before the start of the iteration. Based on these parameters, LTCA under thermal EHL condition will be solved by the multigrid method. Thus, the time varying meshing stiffness $k_m(t)$ and the time varying meshing friction coefficient which are the nonlinear parameters of the dynamic model, are obtained. Then, the governing equations of the face gear dynamic model will be solved by the Runge-Kutta method. Hitherto, the dynamic gear meshing force $F_m(t)$ is obtained. The iterative loop will continue until convergence. And the nonlinear dynamic response can be obtained if the dynamic meshing force satisfies the convergence criterion of 10-3, if not, returning to the step of LTCA under thermal EHL condition.

3.1 Effect of Rotational Speed of Pinion

The pinion speed is one of the key parameters affecting the dynamic response of the face-gear transmission system. The figure 11 shows the bifurcation characteristics of the face-gear transmission system with no dimensional displacement relative to the pinion rotation speed, and there are four types of motion: periodic 1, chaotic, periodic 2, and quasi-periodic, depending on the rotation speed of pinion.

When the rotation speed changes from 4800 rpm to 7600 rpm, the system's dynamic response returns to cycle one motion. This can be clearly seen in the diagram shown in Figure. 11. As the rotational speed increases from 7600 rpm to 8800 rpm, the system's dynamic response results in a period of

ISSN: 2414-1895 DOI: 10.6919/ICJE.202405_10(5).0016

period 2 motion. For rotational speeds below 4000 rpm, the system's dynamic response is periodic one motion. As the rotational speed increases to 4000 rpm but below 4800 rpm, the dynamic response of the system changes from period 1 to chaotic motion. In this region, the bifurcation diagram contains a number of discrete points. There are many points in the Poincaré map, and the FFT spectrum also has multiple peak amplitude.

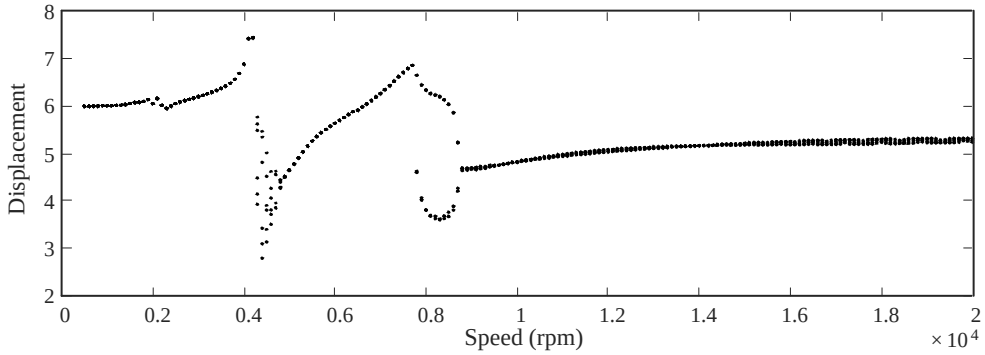

Figure 11. Bifurcation diagram of face-gear transmission system using speed as bifurcation parameter

3.2 Effect of Supporting Stiffness

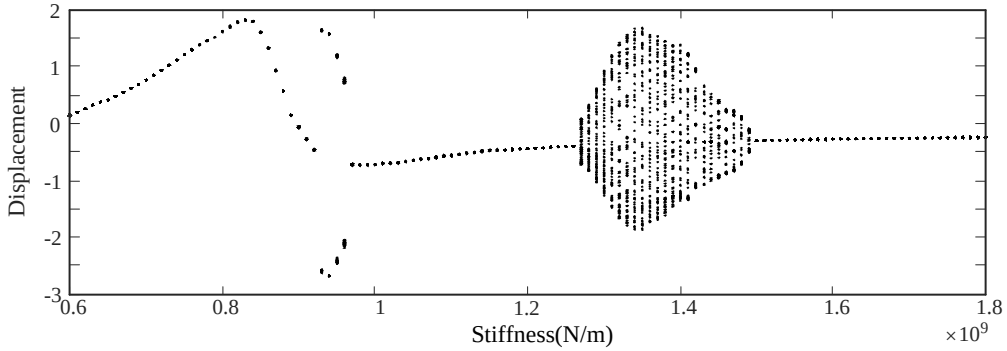

Figre 12. Bifurcation diagram of face-gear transmission system using pinion's supporting stiffness as bifurcation parameter

Pinion support stiffness is another key parameter that affects the dynamic response of the face-gear transmission system. The figure 12 shows the branching characteristics of the face-gear transmission system with no dimensional displacement relative to the support rigidity of the pinion as the rotation speed is 18 when 3000 rpm. As can be seen from the figure, there are three types of motion: period 1, period 2, and chaotic motion.

When the supporting stiffness of pinion is less than 9.3×10^8 N/m, the dynamic response of the system is the movement of period 1. As the support rigidity of the pinion increases from 9.3×10^8 N/m to 9.6×10^8 N/m, the system enters a cycle two motion and maintains its previous state. From 9.6×10^8 N/m to 1.27×10^9 N/m, the system leaves periodic-2 and returns to periodic-1 again. When the supporting stiffness of pinion is increased to 1.27×10^9 N/m, the system dynamic response is changed from periodic-1 motion to chaotic motion, and it is continued until 1.5×10^9 N/m. When the supporting stiffness of pinion is greater than 1.5×10^9 N/m, the system leaves chaotic and return to periodic-1 again.

4. Conclusion

Face-gear transmission systems are primarily used in helicopter transmission systems that require low vibration and high reliability. An accurate dynamic model of the face gear drive is the basis for

ISSN: 2414-1895 DOI: 10.6919/ICJE.202405_10(5).0016

reducing vibration and improving reliability of the helicopter transmission system. Considering backlash, meshing rigidity and meshing friction, this paper presents a dynamic model of a face-gear transmission system under thermal EHL conditions. we used the runge-kutta and multi-grid methods to obtain dynamic responses through iterative loops. The effect of pinion rotation speed and support rigidity on the nonlinear dynamic response of the face-gear transmission system was analyzed numerically.

As described in the above numerical example, the dynamic response of the system with the change of the pinion rotation speed and the support rigidity are as follows: period 1 motion, period 2 motion, Chaos motion and quasiperiodic motion. If the pinion rotation speed is between 4000 rpm and 4800 rpm, the system's dynamic response is chaotic. Moreover, since the rotation speed is 3000 rpm, the support rigidity of pinion is taken as the bifurcation parameter, and the chaotic motion region is determined by the rotation speed, the region of chaotic motion is 1.27×10^9 N/m to 1.5×10^9 N/m. When the system is in a disorderly state of motion, the interaction between the gears becomes complicated and the gear vibration becomes intense, which leads to the failure or instability of the face-gear transmission system. To reduce vibration and increase stability, it is necessary to match the rotation speed and reduction ratio of the pinion and select the appropriate pinion support rigidity based on the optimal design method of the face-gear transmission system.

Overall, the research in this paper not only presents a way to study the nonlinear dynamic properties of face-gear transmission systems, but also provides an idea for vibration control of the main gearbox of future helicopters.

Acknowledgments

This work was supported in part by the “Tangshan Science and Technology Plan Project” of Tangshan (Grant No. 21130216C), in part by the Zhejiang Natural Science Foundation of China (Grant LQ20E050010).

References

[1] G.F. Heath, R.R. Filler, J. Tan. Development of face gear technology for industrial and aerospace power transmission[R]. NASA Report, 2002, NASA/CR-2002-211320.

[2] R.R. Filler, G.F. Heath, S.C. Slaughter, et al. Torque splitting by a concentric face-gear transmission[C]. American Helicopter Society 58th Annual Forum, Montreal, Canada, June 11-13, 2002.

[3] Ning Zhao, Wang Li, Hu Tao, et al. Concentric torque-split face-gear transmission with flexible face gear[J]. Mathematical problems in engineering, vol. 2018, 6568519.

[4] S. Theodossiades, S. Natsiavas. Non-linear dynamics of gear-pair systems with periodic stiffness and backlash[J]. Journal of Sound and Vibration, 2000, 229(2):287-310.

[5] Gou X, Zhu L, Qi C. Nonlinear dynamic model of a gear-rotor-bearing system considering the flash temperature[J]. Journal of Sound Vibration, 2017, 410:187-208.

[6] L. Paouris, R. Rahmani, S. Theodossiades, et al. Inefficiency predictions in a hypoid gear pair through tribodynamics analysis[J]. Tribology International, 2018, 119:631-644.

[7] Guang-Hu, Ru-Peng Z, He-Yun B. Nonlinear dynamical characteristics of face-gear transmission system[J]. Journal of Central South University, 2010, 41(5):1807-1813 (In Chinese).

[8] Chen S, Tang J, Chen W, et al. Nonlinear dynamic characteristic of a face gear drive with effect of modification[J]. Meccanica, 2014, 49(5):1023-1037.

[9] Hu Z, Tang J, Chen S, et al. Coupled translation-rotation vibration and dynamic analysis of face geared rotor system[J]. Journal of Sound and Vibration, 2015, 351:282-298.

[10] Peng Y, Zhao N, Zhang M, et al. Non-Newtonian thermal elastohydrodynamic simulation of helical gears considering modification and misalignment[J]. Tribology International, 2018, 124: 46-60.

ISSN: 2414-1895 DOI: 10.6919/ICJE.202405_10(5).0016

[11] Yang P, Wen S. A generalized Reynolds equation for non-Newtonian thermal elastohydrodynamic lubrication. J Tribol 1990;112:631–6.

[12] Pu W, Wang J, Zhang Y, et al. A theoretical analysis of the mixed elastohydrodynamic lubrication in elliptical contacts with an arbitrary entrainment angle. J Tribol 2014;136(4):041505.

[13] Lin T, Ou H, Li R. A finite element method for 3D static and dynamic contact/impact analysis of gear drives[J]. Computer Methods in Applied Mechanics and Engineering, 2007, 196: 1716-1728.

[14] T. Kiekbusch, D. Sappok, B. Sauer, et al. Calculation of the combined torsional meshing stiffness of spur gears with two- and three-dimensional parametrical FE models[J]. Journal of Mechanical Engineering, 2011, 57(11): 810-818.

[15] S.M. Vijayakar. A combined surface integral and finite element solution for a three-dimensional contact problem [J]. International Journal for Numerical Method in Engineering, 1991, (31): 525-545.

[16] Chang L, Liu G, Wu L. A robust model for determining the mesh stiffness of cylindrical gears[J]. Mechanism and Machine Theory, 2015, 87:93-114.

[17] Hu Z, Tang J, Chen S, Lei D. Effect of mesh stiffness on the dynamic response of face-gear transmission system. ASME. J. Mech. Des. 2013;135(7):071005-071005-7.